

Quantum transport in quasi-periodic lattice systems in presence of Büttiker probes

Madhumita Saha,^{1,*} B. Prasanna Venkatesh,^{2,†} and Bijay Kumar Agarwalla^{1,‡}

¹*Department of Physics, Indian Institute of Science Education and Research Pune,
Dr. Homi Bhabha Road, Ward No. 8, NCL Colony, Pashan, Pune, Maharashtra 411008, India*
²*Department of Physics, Indian Institute of Technology Gandhinagar, Palaj, Gujarat 382355, India*

(Dated: March 1, 2022)

Quasi-periodic lattice systems offer diverse transport properties. In this work, we investigate the environment induced effects on transport properties for quasi-periodic systems, namely the one-dimensional Aubry-André-Harper (AAH) lattice chain and its generalized version (GAAH) by considering the Büttiker probe approach. We first consider voltage probe situation and study the electrical conductance properties in the linear response regime. At zero temperature, we observe enhancement in conductance at all the no-transport regimes, located both inside and outside of the band of the original system, for small probe coupling strength γ with a power-law scaling γ^4 . Whereas, for large probe coupling strengths, the conductance at all Fermi energies is the same and decays as a power-law with scaling $1/\gamma^4$. This particular scaling survives even in the finite-temperature limit. Interestingly, this scaling result is different from the one recently predicted following the local Lindblad master equation approach. The transport eventually becomes diffusive for all energy ranges and in all regimes of the original model for a sufficiently strong coupling with the probes. We further extend our study and consider voltage-temperature probes to analyze the thermoelectric performance of the chain in terms of the figure of merit. We also demonstrate the validity of two recently obtained bounds on thermoelectric efficiency that are tighter than the seminal Carnot bound and express the same in terms of the Onsager's transport coefficients.

I. INTRODUCTION

Quasi-periodic lattice systems reside between a completely disordered system and a periodically ordered system. Such systems can offer a lot of interesting and intriguing transport properties even in low dimensions [1–7]. Recent remarkable experimental realizations of quasi-periodic systems in various cold atom platforms [8–16] have triggered intense theoretical research activities to understand the underlying dynamical and steady-state transport properties. Moreover, some new studies in this context have further revealed the potential of realising highly efficient quantum devices such as quantum rectifiers, thermoelectric engines by carefully exploiting the exotic transport properties [17–20].

The popular quasi-periodic lattice systems, namely, the Aubry-André-Harper (AAH), its generalised version GAAH model and the Fibonacci model [21, 22] have been studied extensively in the context of boundary driven dissipative quantum transport [23–29]. Further studies have started to emerge to understand the environment induced effects on transport [30–37] in such systems. Very recently, following the local Lindblad master equation formalism, the steady-state transport properties due to dephasing noise were analyzed for AAH and Fibonacci models [34]. This approach was however limited to infinite temperature and weak system-environment coupling limit. Following a similar approach, the effect of dephasing noise on transport was studied in presence of

mobility edge [35]. Another recent work [36] focused on understanding thermoelectric transport properties for Fibonacci type model using the first principle Büttiker voltage-temperature probe approach, [38–41] where it was shown that noise induced processes can lead to a better thermoelectric performance in certain regimes of transport. Note that, such a Büttiker probe technique was used extensively in the past to understand effective many-body transport properties in setups like molecular junctions [42–49], quantum dots [50], lattice models of oscillators [51–53] etc.

In this work, we analyse how transport properties in AAH and its generalized version i.e., the GAAH lattice models are modified in presence of the Büttiker probes. We implement both the voltage probe and voltage-temperature probe techniques and explore charge transport and thermoelectric heat-to-work conversion properties in the linear-response regime. For the thermoelectric setup, we further asses and compare the recently obtained tighter bounds on efficiency following the thermodynamic uncertainty relations [54] and the bound obtained in Ref. [55].

We organize the paper as follows: in section II, we introduce the AAH and GAAH lattice models and then briefly describe the theoretical aspects of the Büttiker probe approach and how to obtain charge conductance in the the linear response regime. In section III, we present the numerical results examining the behavior of conductance in the voltage probe setting. In section IV, we extend our study to voltage-temperature probes and study thermoelectric performance for the AAH chain and furthermore asses the recently obtained tighter bounds on efficiency by expressing these bounds in terms of the Onsager's transport coefficients. Finally we conclude with a

* madhumita.saha@acads.iiserpune.ac.in

† prasanna.b@iitgn.ac.in

‡ bijay@iiserpune.ac.in

discussion summarizing our results in section V.

II. MODEL AND THEORY

A. Model Hamiltonian

We consider an out-of-equilibrium one-dimensional quasi-periodic lattice chain that is connected at its two ends to two thermo-chemical reservoirs. These reservoirs are always maintained at fixed chemical potentials and temperatures. Since we are interested in investigating the environment induced effects on the central quasi-periodic lattice chain, we connect uniform and independent local reservoirs, i.e., Büttiker probes to each lattice site. The Hamiltonian for the entire setup is then given as

$$H = H_S + H_B + H_{SB} + H_P + H_{PS}, \quad (1)$$

where H_S represents a quasi-periodic chain with Hamiltonian

$$H_S = \sum_i \epsilon_i c_i^\dagger c_i + t \sum_i (c_{i+1}^\dagger c_i + c_i^\dagger c_{i+1}). \quad (2)$$

Here $c_i^\dagger (c_i)$ is the creation (annihilation) operator for the electron at the i th site. Here we consider only the nearest neighbour hopping with hopping amplitude t . The site dependent onsite potential ϵ_i mimics a quasi-periodic potential which for the generalized Aubry-André-Harper (GAAH) model is given as,

$$\epsilon_i = \frac{2\lambda \cos[2\pi bi + \Phi]}{1 + \alpha \cos[2\pi bi + \Phi]}, \quad (3)$$

where λ represents the strength of the potential, b is an irrational number which makes the potential quasi-periodic, and Φ is the phase factor that generates different configurations of the quasi-periodic potential. For, $\alpha = 0$, this model reduces to the AAH model [1, 2]. For AAH model, all the single particle eigenstates are delocalized for $\lambda < 1$ and exponentially localized for $\lambda > 1$ [1] and at $\lambda = 1$ all the states are critical, i.e., neither localized nor delocalized. As a result, the particle transport goes from ballistic to exponentially suppressed as the value of λ is tuned from delocalized to localized regime and at the critical point the transport shows anomalous behaviour with sub-diffusive scaling of transport coefficient with system size [24, 25].

For non-zero α , i.e., for the GAAH model, the system possesses a single-particle mobility edge which can be obtained analytically, $E = 2 \operatorname{sgn}(\lambda)(1 - |\lambda|)/\alpha$ [4] where E corresponds to a single particle energy eigenvalue. In this case, all the single particle eigenstates with energy less than E are extended/delocalized while those states with energy higher than E are localized. Hence, when E falls within the spectrum, it is a mobility edge.

In Eq. (1), $H_B = H_L + H_R$ represents the Hamiltonian for the left and the right reservoirs. For this study, we

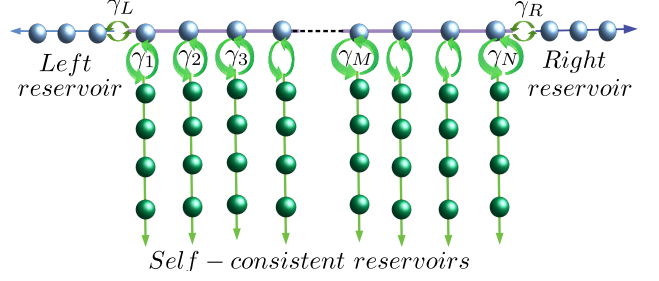


FIG. 1. (Color online): Schematic of a one-dimensional lattice chain with the first and the last sites of the chain are connected to the left and the right reservoirs, respectively. These reservoirs have different chemical potentials that induce current in the chain. In addition, each lattice site is attached to a local reservoir which we refer here as the Büttiker probe. The probes, left and right reservoirs are all modelled as 1-D ordered semi-infinite tight binding chains.

model these reservoirs as 1-D tight-binding ordered semi-infinite chain with Hamiltonian,

$$H_L = \epsilon_0 \sum_k a_k^\dagger a_k + t_0 \sum_k a_{k+1}^\dagger a_k + \text{H.c.}, \quad (4)$$

$$H_R = \epsilon_0 \sum_k b_k^\dagger b_k + t_0 \sum_k b_{k+1}^\dagger b_k + \text{H.c.}, \quad (5)$$

with a_k and b_k correspond to the annihilation operators of the k th sites for left and right baths, respectively. For simplicity, we choose the same onsite and the same hopping parameters for both the baths. The term $H_{SB} = H_{SL} + H_{SR}$ represents the coupling between the system and the baths and is responsible for the charge transfer across the system. It is specified by,

$$H_{SL} = \gamma_L a_1^\dagger c_1 + \text{H.c.}, \quad (6)$$

$$H_{SR} = \gamma_R b_1^\dagger c_N + \text{H.c.}, \quad (7)$$

where the left (right) bath is coupled to the first (N -th) site of the quasi-periodic lattice chain with coupling strength γ_L (γ_R).

As mentioned before, the dephasing and dissipation effects within the central lattice chain can be modelled phenomenologically by connecting local reservoirs (probes) at each lattice site. As done for the left and the right reservoirs, for this study, we model each probe also as a 1D tight-binding ordered semi-infinite chain. The total Hamiltonian for the probes is given as $H_P = \sum_{i=1}^N H_P^i$ with each probe Hamiltonian is given by

$$H_P^i = \sum_j [\epsilon_0 d_{ij}^\dagger d_{ij} + t_0 d_{ij+1}^\dagger d_{ij} + \text{H.c.}] \quad (8)$$

Correspondingly, the coupling Hamiltonian between the i -th probe and the central system is given as,

$$H_{PS}^i = \gamma c_i^\dagger d_{i1} + \text{H.c.}, \quad (9)$$

where the first site of each probe is coupled to the i -th site of the central system with coupling strength γ , which is chosen to be the same for all the probes.

B. Theory

We employ the non-equilibrium Green's function (NEGF) approach [56–61] to investigate end-to-end transport through the central quasi-periodic chain. In presence of the two-baths at the ends and the Büttiker probes, one can obtain the retarded Green's function for the central system as,

$$G^r(\epsilon) = \left[\epsilon I - H_C - \Sigma_L^r(\epsilon) - \Sigma_R^r(\epsilon) - \sum_{i=1}^N \Sigma_P^r(\epsilon)^i \right]^{-1} \quad (10)$$

where I is the $N \times N$ Identity matrix with N being the number of lattice sites of the central system and is also equal to the total number of probes attached to the central lattice. H_C represents $N \times N$ single particle hamiltonian corresponding to H_S . $\Sigma_\alpha^r(\epsilon)$, $\alpha = L, R, P$ is the self-energy associated with the α -th bath. Note that the effects of the baths, including the probes, are additive in the self-energy. Since we have chosen the baths and the Büttiker probes as semi-infinite ordered tight-binding chains, the self-energies in this case can be obtained analytically and given by [62],

$$\Sigma_\alpha^r(\epsilon) = \frac{\gamma_\alpha^2}{2t_0^2} \left[\epsilon - i\sqrt{\epsilon^2 - 4t_0^2} \right], \quad \alpha = L, R, P. \quad (11)$$

where $\epsilon_0 = 0$, and $\gamma_P = \gamma$. Before we proceed further, let us fix some notations. We identify the index n with the probe terminals, ν to identify the left and the right reservoirs and use index α to count all the leads. Since the entire setup is fully quadratic, the average charge current in the steady state flowing out of the ν -th reservoir is given by the famous Landauer-Buttiker formula [59],

$$I_\nu = \frac{e}{2\pi} \sum_\alpha \int_{-\infty}^{\infty} d\epsilon \mathcal{T}_{\nu\alpha}(\epsilon) \left(f_\nu(\epsilon) - f_\alpha(\epsilon) \right), \quad \nu = L, R. \quad (12)$$

Here $f_\alpha(\epsilon) = (1 + e^{\beta(\epsilon - \mu_\alpha)})^{-1}$ is the Fermi distribution function of α -th terminal with inverse temperature β and chemical potential μ_α . $\mathcal{T}_{\nu\alpha}(\epsilon)$ is the transmission probability for an electron to flow from ν -th terminal to α -th terminal through the quasi periodic system. The transmission probabilities can be computed using the Green's function of the central system and the self-energy of the baths and expressed as,

$$\mathcal{T}_{\nu\alpha}(\epsilon) = \text{Tr} \left[\Gamma_\nu(\epsilon) G^r(\epsilon) \Gamma_\alpha(\epsilon) G^a(\epsilon) \right], \quad (13)$$

where $\Gamma_\alpha(\epsilon) = -2 \text{Im}[\Sigma_\alpha^r(\epsilon)]$.

One can similarly compute the charge current flowing out of the n th probe which is also given by the Landauer-Buttiker formula,

$$I_n = \frac{e}{2\pi} \sum_\alpha \int_{-\infty}^{\infty} d\epsilon \mathcal{T}_{n\alpha}(\epsilon) \left(f_n(\epsilon) - f_\alpha(\epsilon) \right), \quad n = 1, 2, \dots, N. \quad (14)$$

In what follows, we first analyze the effect on end-to-end conductance properties by considering the local reservoirs as voltage probes and thus set the net charge current flowing out of each probe to zero, i.e., $I_n = 0$ for $n = 1, 2, \dots, N$ in Eq. (14). Imposing this constraint for each probe allows one to simulate both elastic dephasing and inelastic dissipative processes in the central lattice chain. In section IV, we further extend the above study by considering the local reservoirs as voltage-temperature probes and demand vanishing charge and heat currents from each probe which then allow us to simulate inelastic but non-dissipative scattering processes. Under this setting, we study thermoelectric heat-to-work conversion properties and the recently obtained tighter bounds on thermoelectric efficiency.

C. Voltage probe technique in linear response regime

In this sub-section, we first focus on the voltage probe technique by considering the temperature of the end reservoirs and the probes to be the same. The different chemical potential of the two end reservoirs drive a steady-state current in the chain. We impose the zero charge current condition from each probe which in turn fixes the local chemical potential of each probe. We concentrate on the linear response regime and expand the Fermi-distribution function around the equilibrium chemical potential ϵ_F and inverse temperature β as,

$$f_K(\epsilon) = f_{\text{eq}}(\epsilon) - \frac{\partial f_{\text{eq}}(\epsilon)}{\partial \epsilon} (\mu_K - \epsilon_F). \quad (15)$$

The derivative of the Fermi function is also evaluated at ϵ_F . Now putting Eq. (15) in Eq (14), for each n and setting $I_n = 0$, $n = 1, 2, \dots, N$, we receive a set of N linear equations for the chemical potential of each probe n of the form,

$$\mu_n = \mu_R + \sum_{j=1}^N \left[\mathcal{W}_{nj}^{-1} \int_{-\infty}^{\infty} \mathcal{T}_{jL}(\epsilon) \left(-\frac{\partial f_{\text{eq}}(\epsilon)}{\partial \epsilon} \right) d\epsilon \right] (\mu_L - \mu_R), \quad \forall n = 1, 2, \dots, N \quad (16)$$

Here \mathcal{W} is an $N \times N$ matrix given as,

$$\mathcal{W} = \begin{pmatrix} \sum_{\alpha \neq 1} \int_{-\infty}^{\infty} \mathcal{T}_{1,\alpha}(\epsilon) \left(-\frac{\partial f_{\text{eq}}(\epsilon)}{\partial \epsilon} \right) d\epsilon & -\int_{-\infty}^{\infty} \mathcal{T}_{1,2}(\epsilon) \left(-\frac{\partial f_{\text{eq}}(\epsilon)}{\partial \epsilon} \right) d\epsilon & -\int_{-\infty}^{\infty} \mathcal{T}_{1,3}(\epsilon) \left(-\frac{\partial f_{\text{eq}}(\epsilon)}{\partial \epsilon} \right) d\epsilon & \dots \\ -\int_{-\infty}^{\infty} \mathcal{T}_{2,1}(\epsilon) \left(-\frac{\partial f_{\text{eq}}(\epsilon)}{\partial \epsilon} \right) d\epsilon & \sum_{\alpha \neq 2} \int_{-\infty}^{\infty} \mathcal{T}_{2,\alpha}(\epsilon) \left(-\frac{\partial f_{\text{eq}}(\epsilon)}{\partial \epsilon} \right) d\epsilon & -\int_{-\infty}^{\infty} \mathcal{T}_{2,3}(\epsilon) \left(-\frac{\partial f_{\text{eq}}(\epsilon)}{\partial \epsilon} \right) d\epsilon & \dots \\ -\int_{-\infty}^{\infty} \mathcal{T}_{3,1}(\epsilon) \left(-\frac{\partial f_{\text{eq}}(\omega)}{\partial \epsilon} \right) d\omega & -\int_{-\infty}^{\infty} \mathcal{T}_{3,2}(\epsilon) \left(-\frac{\partial f_{\text{eq}}(\epsilon)}{\partial \epsilon} \right) d\epsilon & \sum_{\alpha \neq 3} \int_{-\infty}^{\infty} \mathcal{T}_{3,\alpha}(\epsilon) \left(-\frac{\partial f_{\text{eq}}(\epsilon)}{\partial \epsilon} \right) d\epsilon & \dots \\ \dots & \dots & \dots & \dots \end{pmatrix}.$$

Given the local chemical potentials μ_n in Eq. (16), we can compute the electrical conductance G for this setup as, $G = I_R/\Delta V$ with $\Delta V = (\mu_R - \mu_L)/e$ being the applied bias voltage,

$$G = G_0 \int_{-\infty}^{\infty} d\epsilon \left(-\frac{\partial f_{\text{eq}}(\epsilon)}{\partial \epsilon} \right) \left[\mathcal{T}_{R,L}(\epsilon) + \int_{-\infty}^{\infty} d\epsilon' \sum_{nj} \mathcal{T}_{Rn}(\epsilon) \mathcal{W}_{nj}^{-1} \mathcal{T}_{jL}(\epsilon') \left(-\frac{\partial f_{\text{eq}}(\epsilon')}{\partial \epsilon'} \right) \right] \quad (17)$$

where $G_0 = e^2/2\pi\hbar$ is the universal quantum electrical conductance. The second term in the above expression reflects the change in the conductance due to the probes and mimics various type of incoherent or phase breaking processes. In the zero temperature limit ($\beta \rightarrow \infty$) [51], the above equation simplifies drastically as $\frac{\partial f_{\text{eq}}(\epsilon)}{\partial \epsilon} = -\delta(\epsilon - \epsilon_F)$, and the conductance can be expressed simply in terms of an effective transmission function $G = G_0 \mathcal{T}_{\text{eff}}(\epsilon_F)$, where

$$\mathcal{T}_{\text{eff}}(\epsilon_F) = \mathcal{T}_{RL}(\epsilon_F) + \sum_{nj} \mathcal{T}_{Rn}(\epsilon_F) \mathcal{W}_{nj,0}^{-1} \mathcal{T}_{jL}(\epsilon_F) \quad (18)$$

In the above equation, $\mathcal{W}_{nj,0}$ denotes the matrix elements of \mathcal{W} computed in the zero temperature limit. Interestingly, for $\beta \rightarrow \infty$, the local probes are exactly equivalent to the dephasing probes as the zero particle current condition from Eq. (14) is now satisfied for each energy.

III. RESULTS- VOLTAGE PROBE

We now present the numerical results for conductance at both zero and finite temperatures. Since the zero temperature calculation does not require any numerical integration to be performed, one can therefore simulate large system sizes. Here we report results upto $N = 1597$. Unless otherwise stated, for all the numerical calculations we choose $\epsilon_0 = 0$, $t_0 = 3$, $t = 1$, $\gamma_L = \gamma_R = 1$. Note that, to reduce the number of parameters in the problem, we have chosen a spatially uniform situation for the probes by setting $\gamma_n = \gamma$ for all $n = 1, 2, \dots, N$. We also stress that in the following discussions by coherent transport we imply transport through quasi-periodic lattice in absence of the probes ($\gamma_n = 0$).

In Fig. 2 we first display the effects of voltage probes in three different transport regimes of the AAH model corresponding to three different λ values: ballistic ($\lambda = 0.5$, Fig. (2(a))), critical ($\lambda = 1.0$, Fig. (2(b))) and localized ($\lambda = 1.2$, Fig. (2(c))) at zero temperature. In absence of probes, in all three regimes of the AAH model, there

are energy values located within and outside the band of the lattice system (the vertical dotted lines in Fig. (2) represent the band edges of the central lattice chain), at which no significant transport takes place due to the absence of bare energy states of the central system. However, once the voltage probes are attached, the transport properties in all the regimes change significantly. In particular, in presence of probes, finite transport is induced for all Fermi energies that corresponds to no-transport in the coherent case. Moreover, here we observe that for these particular energies, the value of conductance increases with increasing system-probe coupling γ . In contrast, the energy values for which significant transport is already present in the coherent limit, the conductance display non-monotonic behavior with increasing γ . Note that, in the localized regime (Fig. (2)(c)), as there is essentially no transport for any ϵ_F in the coherent limit, attaching probes always induces finite conductance for all Fermi energies.

To establish this behaviour more explicitly, we choose different ϵ_F 's corresponding to no-transport and transport cases in the coherent limit, and plot in Fig. 3(a)-(c) the zero-temperature conductance as a function of the coupling strength γ . Interestingly, as mentioned before, for no-transport energies, the conductance increases with γ but as a power-law with scaling γ^4 upto a critical value $\gamma_c \sim t, \gamma_L, \gamma_R$. In contrast, no particular scaling is observed for the transport energies where attaching probes may increase or decrease the value of conductance. Note that, for the critical λ (Fig. 3(b)), as the eigenstates of the bare system are not completely delocalized, increase in conductance is observed even for Fermi energies that corresponds to finite transport. Interestingly, beyond the critical value of the probe coupling, i.e., $\gamma_c > t, \gamma_L, \gamma_R$, the conductance becomes independent of λ and is equal for all ϵ_F 's and more importantly decays as a power law $1/\gamma^4$. Note that, this scaling result is different than the one recently predicated following the local Lindblad master equation approach where the analysis was carried out in the infinite temperature limit with scaling given as $1/\gamma^2$ [34]. In Fig. (3)(d)-(f) we extend these results to finite-temperature limit. We observed that, at high temperature $T = 200$, the conductance value is the same for all Fermi energies, implying a flat transmission spectrum with ϵ_F . Below γ_c , the contributions to conductance come from all energies that reside within the energy window of width $k_B T$ around ϵ_F and as a result no particular scaling with γ is observed. However, interestingly, for large γ the conductance scaling remains the same as the zero temperature case.

We next present the scaling of the conductance with

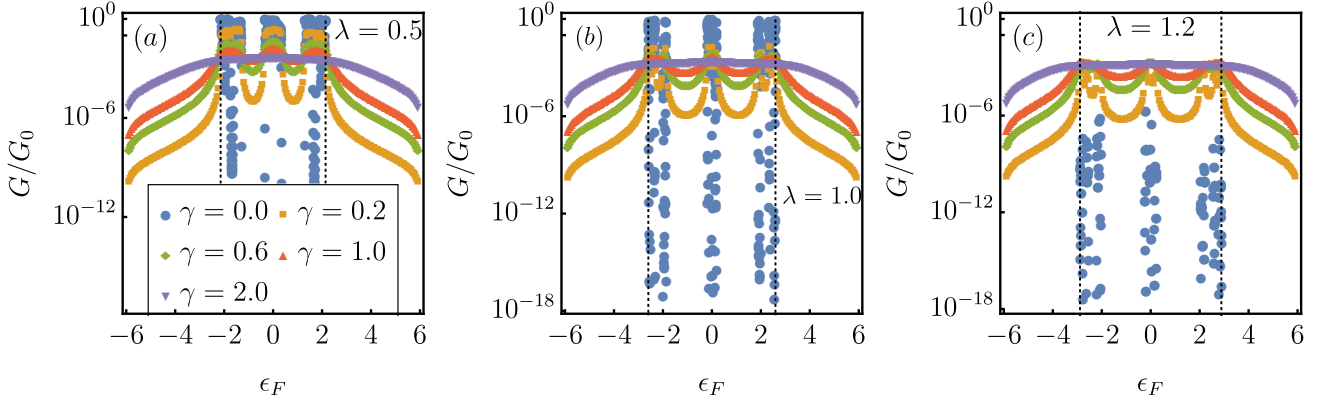


FIG. 2. (Color online): Plots for zero-temperature conductance in absence and presence of Büttiker voltage probes for the AAH model in three different transport regimes. In the coherent regime (absence of probes), AAH model displays delocalized ($\lambda < 1$), critical ($\lambda = 1$), and localized ($\lambda > 1$) phases depending on the strength λ . Here, we display the effect of voltage probes on transport. The vertical dotted lines represent the band edges of the AAH model. Here, the system size is taken as $N = 200$.

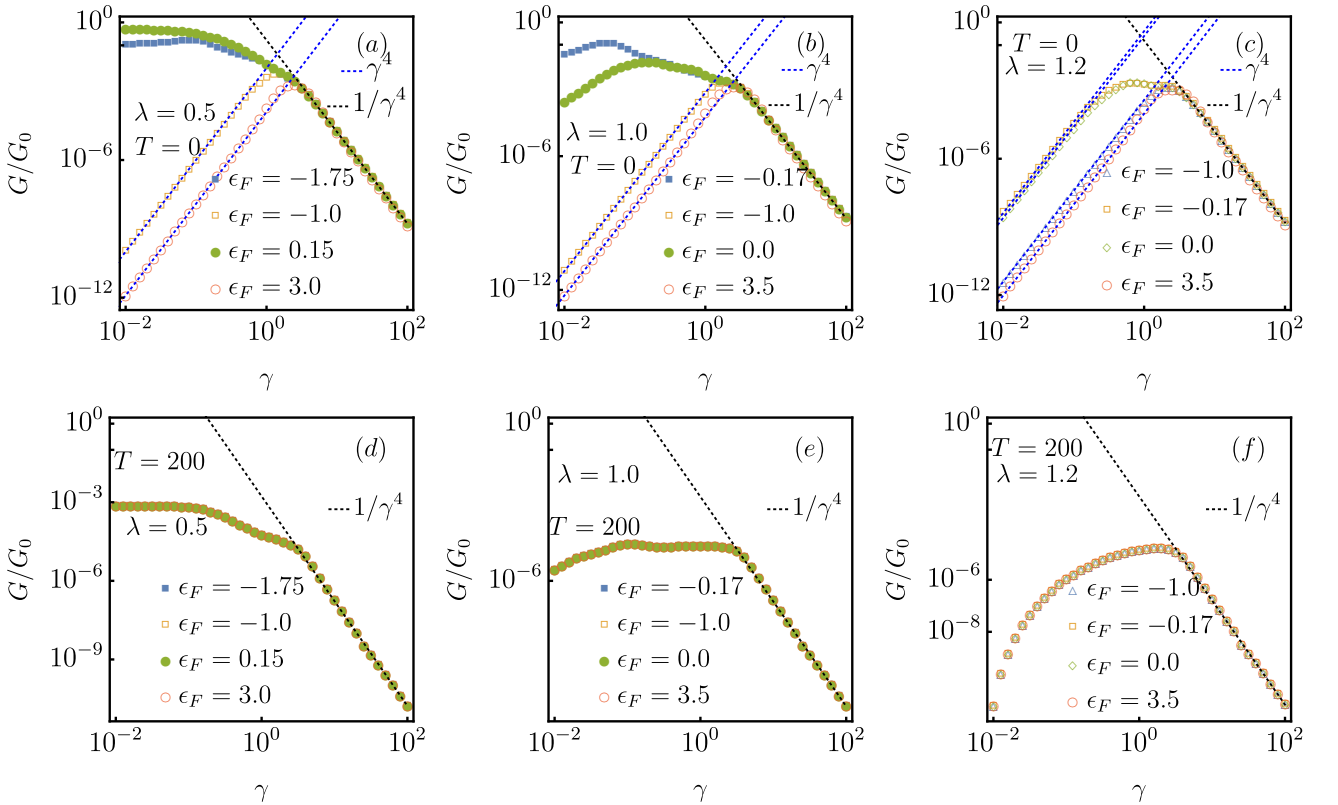


FIG. 3. (Color online): Plots for zero-temperature conductance as a function of system-probe coupling strength γ in different transport regimes of AAH model at different Fermi energies. Here, the system size is taken as $N = 200$.

the system size N . In Fig. 4(a)-(c), we display the crossover from various transport regimes in the coherent limit scaling to a diffusive limit $G \sim N^{-1}$. We note that for finite system size, with sufficiently strong incoherent effects induced by the probes, the transport eventually becomes diffusive for all λ values. For weak γ , the conductance however display a crossover from the coherent

limit scaling to a diffusive scaling and the corresponding crossover length varies strongly depending on whether the transport is ballistic, sub-diffusive or localized in the coherent regime. As an example, for the same γ value ($\gamma = 0.3$) in the localized case (4(c)), the crossover takes place at a small system size $N \sim 30$ compared to the ballistic case $N \sim 200$. This fact corroborates with the

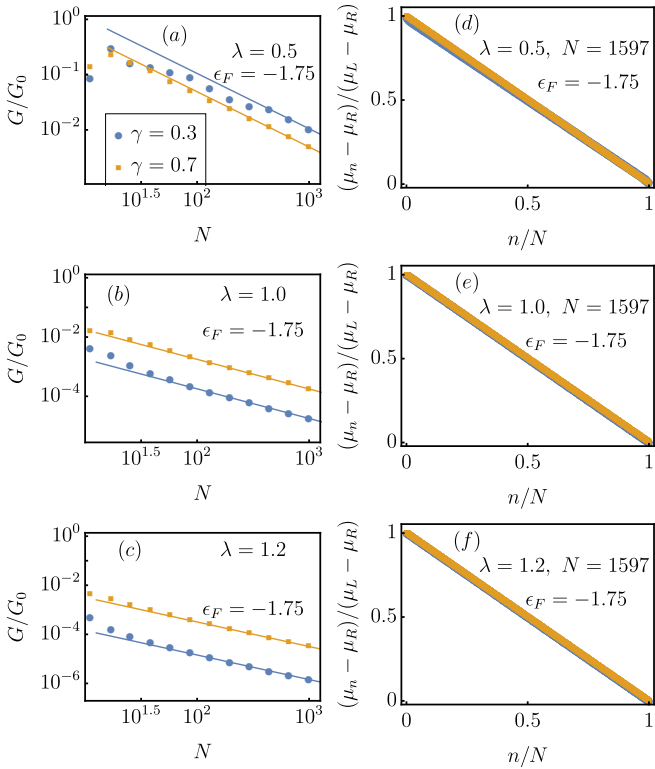


FIG. 4. (Color online): Plots (a)-(c) show crossover to diffusive transport regime from ballistic ($\lambda = 0.5$), sub-diffusive ($\lambda = 1.0$) and exponentially localized ($\lambda = 1.2$) phases, respectively, in presence of voltage probes at zero temperature. The solid lines represent diffusive $1/N$ scaling. Plots (d)-(f) show the corresponding chemical potential profiles. The linear chemical potential profile ensures that the transport is diffusive. We show results for two different γ values.

predictions in Ref. ([34]). For a fixed λ , with increasing γ , the crossover length shrinks and a diffusive scaling sets in. In Fig. 4(d)-(f), we display the corresponding chemical potential profile in the lattice chain which shows a clear linear behavior in presence of probes, indicating a diffusive transport.

It is important to note that, in the critical regime of the coherent AAH model ($\gamma = 0$), the conductance can display different sub-diffusive scalings depending on the choice of the system size [24, 27]. For example, at $\lambda = 1$ (critical regime), if the system size is considered as a Fibonacci number (we have considered here b as the ratio of two Fibonacci numbers), a sub-diffusive scaling $N^{-1.26}$ is observed whereas for the case of non-Fibonacci numbers the sub-diffusive scaling $N^{-1.4}$ is observed. It is interesting to see that, in presence of probes, for both cases, a crossover from sub-diffusive to diffusive regime is observed, as shown in Fig. 5. Furthermore we observe that for all λ , interestingly, the crossover length from coherent to diffusive transport is independent of the temperature, as displayed in Fig. 6.

Since the transport eventually becomes diffusive in presence of probes, in the diffusive regime we define the

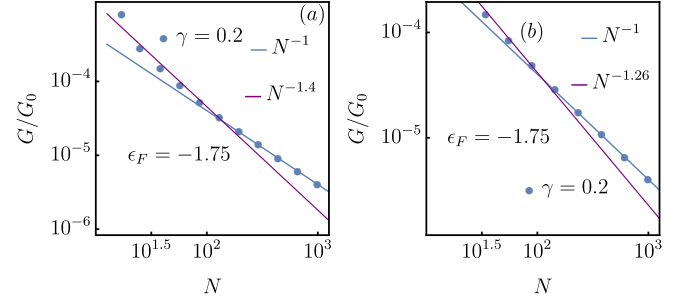


FIG. 5. (Color online): Crossover from sub-diffusive behaviour to diffusive behaviour for $\gamma = 0.2$ at the critical point ($\lambda = 1$) of AAH model at zero temperature. Depending on the chosen system size one can see crossover to N^{-1} from different sub-diffusive scaling. In (a), the chosen system sizes do not correspond to Fibonacci numbers and in (b), the system sizes correspond to Fibonacci numbers.

electrical conductivity $\sigma = \lim_{N \rightarrow \infty} \sigma(N)$ with $\sigma(N) = NG$ being the finite-size conductivity. In Fig. 7, we display σ as a function of λ , the strength of the quasi-periodic potential. Interestingly, the conductivity σ strongly depends on λ with the value monotonically decreasing with increasing λ . This implies that even though the system is in the diffusive regime, the conductivity is still larger in $\lambda < 1$ regime in comparison to $\lambda > 1$ regime. However, for large γ , the quasi-periodic nature of the lattice is smeared out by the probe coupling and conductivity becomes essentially insensitive to the value of λ .

We next briefly discuss the results for the generalized AAH i.e., the GAAH model (see Eq. (3)). In this case, we observe similar trends in conductance to the one observed for the AAH model. As done in Fig. 2, in Fig. 8, we plot G as a function of ϵ_F in presence of mobility edge. For the chosen parameters in our simulations, all the states above (below) the mobility edge are localized (delocalized). As can be seen in Fig. 8(b), in all the non-transport regimes, due to the coupling with probes, there is enhancement of G up to a critical $\gamma_c \sim t, \gamma_L, \gamma_R$ with conductance increasing as γ^4 and thus displaying universality. Furthermore, beyond γ_c , similar to the AAH case, the G decreases as $1/\gamma^4$. In Fig. 8(c) and (d), we show that for this model also, the transport eventually becomes diffusive at all regimes.

IV. RESULTS- VOLTAGE-TEMPERATURE PROBE TECHNIQUE AND THERMOELECTRIC PERFORMANCE

In this section we extend our study to voltage-temperature probe that enables us to investigate thermoelectric properties. In this case, the left and right reservoirs are kept at fixed chemical potentials (μ_L, μ_R) and temperatures (T_L, T_R). Next we impose the voltage-temperature probe conditions of zero particle and heat

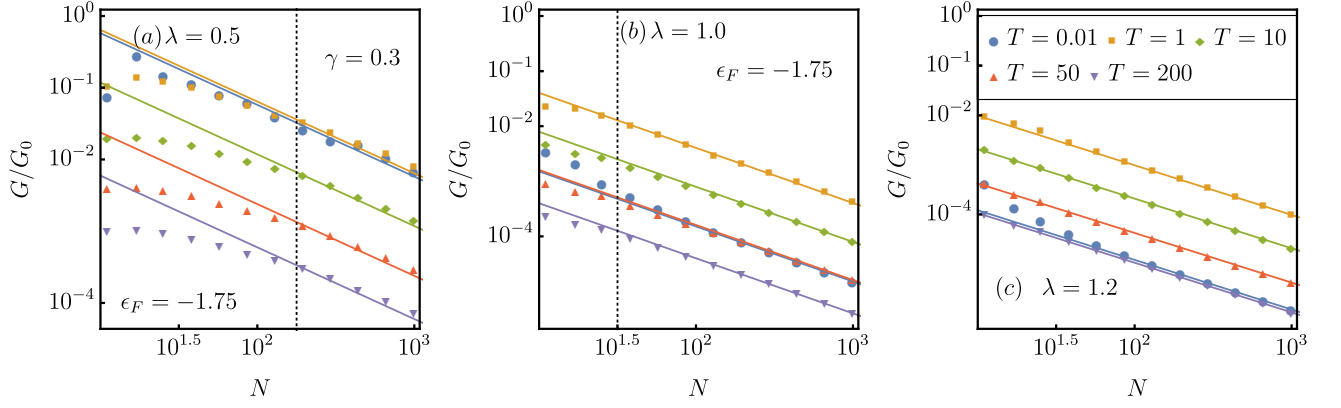


FIG. 6. (Color online) Plots (a)-(c) shows crossover to diffusive regime at finite temperatures for probe coupling strength $\gamma = 0.3$. The solid lines represent diffusive $1/N$ scaling. The vertical dotted lines represent the system size after which the diffusive transport sets further indicating temperature independent system-size crossover.

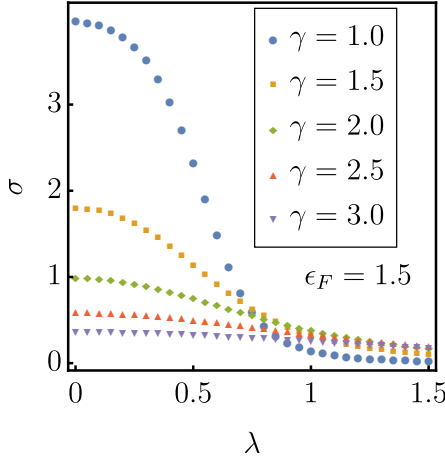


FIG. 7. (Color online): Plot for electrical conductivity $\sigma = \lim_{N \rightarrow \infty} NG$ in the diffusive regime as a function of quasi-periodic lattice strength λ for different values of γ .

currents flowing out of each probe and thereby determine the chemical potential and temperature of each probe. Thus, we set,

$$I_n = \frac{e}{\hbar} \sum_{\alpha} \int_{-\infty}^{\infty} d\epsilon \mathcal{T}_{n\alpha}(\epsilon) (f_n(\epsilon) - f_{\alpha}(\epsilon)) = 0, \\ Q_n = \frac{1}{\hbar} \sum_{\alpha} \int_{-\infty}^{\infty} d\epsilon (\epsilon - \mu_n) \mathcal{T}_{n\alpha}(\epsilon) (f_n(\epsilon) - f_{\alpha}(\epsilon)) = 0. \\ n = 1, 2, \dots, N \quad (19)$$

Once again, we focus on the linear response regime and obtain μ_n and T_n for the probes in terms of μ_L, μ_R, T_L , and T_R . Finally, we can write the particle (I_R) and heat currents (Q_R) flowing out from the right bath as,

$$\langle I_R \rangle = G \Delta V + G S \Delta T \\ \langle Q_R \rangle = G \Pi \Delta V + (K + G S \Pi) \Delta T \quad (20)$$

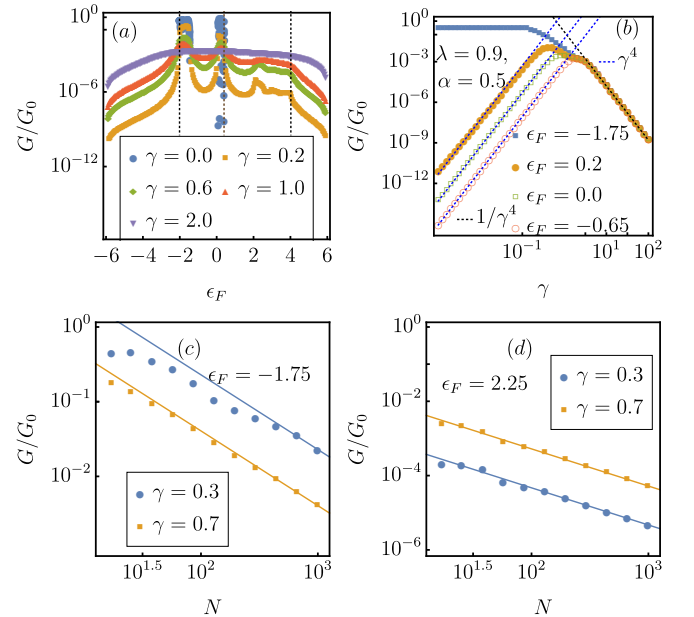


FIG. 8. (Color online): Plot (a) displays the effect of probes on transport. The dotted vertical lines at the two ends represent the band edges and the vertical line in the middle represents the mobility edge. Plot (b) displays conductance as a function of γ for different Fermi energies. Plots (c)-(d) show the crossover to diffusive regime from both no-transport and transport regimes in presence of probes.

where G is the electrical conductance, K is the thermal conductance, S is the Seebeck coefficient and Π is the Peltier coefficient. Here $\Delta V = (\mu_R - \mu_L)/e$ and $\Delta T = T_R - T_L$. All of the above transport coefficients depend on the average temperature $T = (T_L + T_R)/2$ and average chemical potential $\epsilon_F = (\mu_L + \mu_R)/2$. In presence of the probes, we numerically verified the Onsager's reciprocity relation, given by $\Pi = TS$. Note

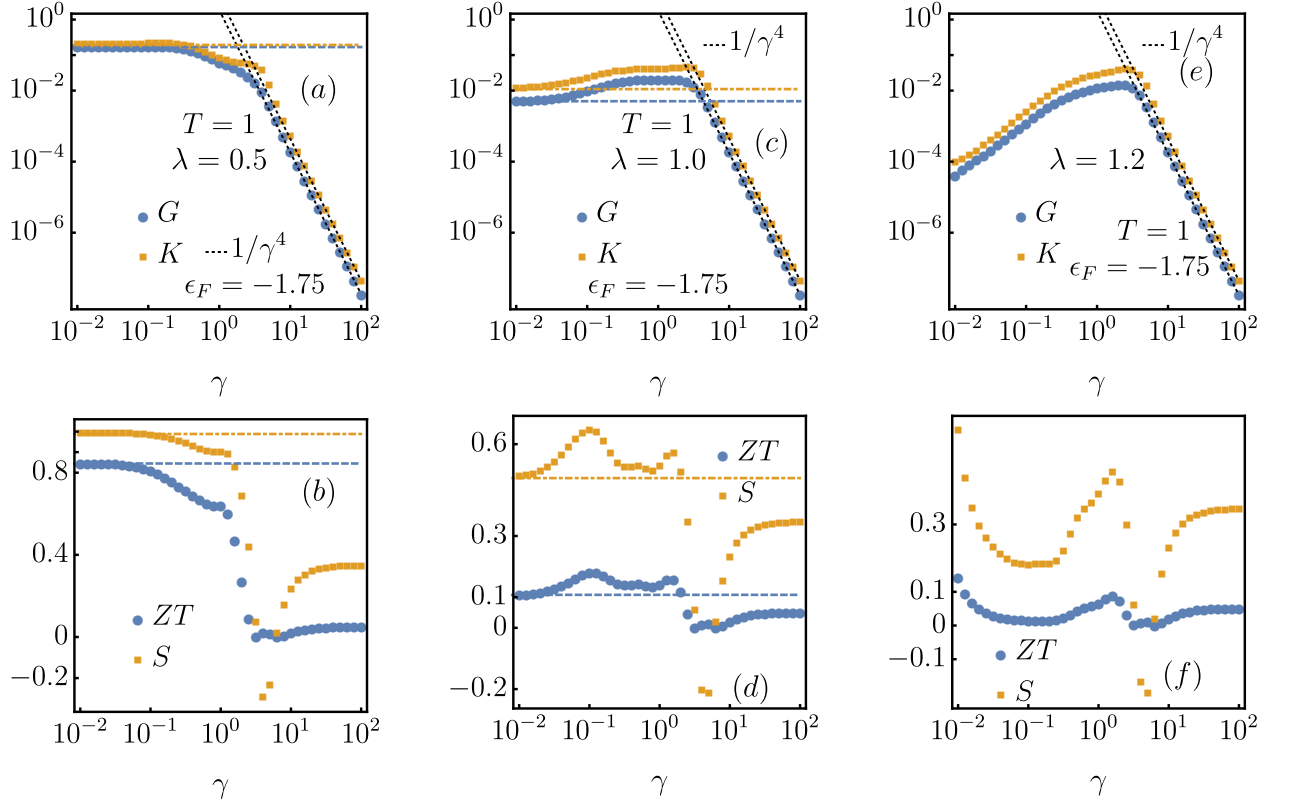


FIG. 9. (Color online): Plots (a)-(f) display the various transport coefficients and the ZT for the AAH model as a function of probe coupling strength γ in presence of voltage-temperature probes. The horizontal lines in (a)-(d) represent the values of transport coefficients in the coherent limit ($\gamma = 0$).

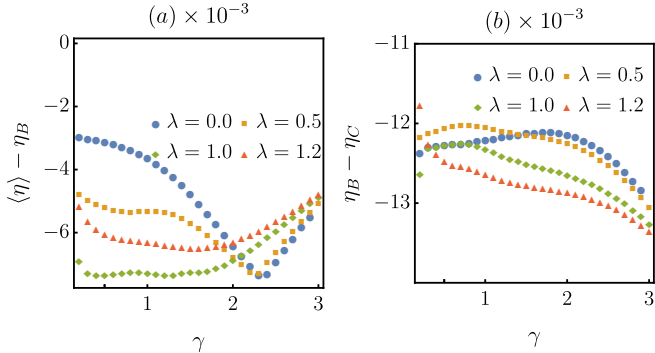


FIG. 10. (Color online): Plots for (a) tighter bound on mean efficiency i.e., $\langle\eta\rangle - \eta_B$ and (b) the bound $\eta_B - \eta_C$ as functions of γ for different values of λ . The parameters are $N = 34$, $T = 1$, $\Delta T = 0.2$, $\mu = -1.75$, $\mu_R - \mu_L = -0.001$.

that in order to compute G , Π , S and K in presence of voltage-temperature probes, we first consider $\Delta T = 0$ and extract the transport coefficients G and Π and next consider $\Delta V = 0$ to extract the other two coefficients S and K . Now in order to realize a thermoelectric engine, we set $\mu_L > \mu_R$ and $T_R > T_L$ and demand $\langle I_R \rangle > 0$ and $\langle Q_R \rangle > 0$ i.e., heat absorbed from the hot right bath

induces particle current against the chemical potential difference. The average power output is then given as $\langle P \rangle = -\Delta V \langle I_R \rangle$ and as a result, the average thermoelectric efficiency of the engine is given by $\langle \eta \rangle = \frac{\langle P \rangle}{\langle Q_R \rangle}$. In the linear response regime, the maximum thermoelectric efficiency $\langle \eta \rangle_{\max}$ is characterised by a single dimensionless quantity, the thermoelectric figure of merit $ZT = \frac{GS^2}{K}T$ and is given as,

$$\langle \eta \rangle_{\max} = \eta_C \frac{\sqrt{ZT + 1} - 1}{\sqrt{ZT + 1} + 1} \quad (21)$$

where $\eta_C = \Delta T/T$ is the Carnot efficiency in the linear response regime. In Fig. 9 (a)-(f), we display the behaviour of various transport coefficients and ZT for the AAH model as a function of γ , for different values of λ . Interestingly, like the electrical conductance G , the thermal conductance K also shows a similar scaling $1/\gamma^4$ at strong probe coupling in all regimes. The Seebeck coefficient however does not display any such scaling. Starting in the $\lambda < 1$ regime, the values for both G and K are always lower than that in the coherent limit, whereas probe induced enhancement can be seen in both $\lambda = 1$ and $\lambda > 1$ regimes (Fig. 9 (c)-(e)). As a result, ZT decays with increasing γ in the $\lambda < 1$ regime but in the other two regimes an enhancement in ZT value, compared to

the coherent limit, is seen for some values of γ . Note that the overall value of ZT however always remains higher for $\lambda < 1$ in comparison to the other two regimes. For large γ , all three regimes converge to the same ZT value.

We next move on to analyze two recently obtained universal bounds [54, 55] for the mean efficiency in the context of our thermoelectric engines. Interestingly, these universal bounds are found to be tighter than the seminal Carnot bound and are written in terms of the current fluctuations. One of the bounds emerge from the recently discovered thermodynamic uncertainty relations (TURs) [55, 63, 64] which is a trade-off relation between power, efficiency and power fluctuation. In the context of thermoelectric engine, operating in the linear response regime, following the TURs we obtain the bound on mean efficiency as,

$$\langle \eta \rangle \leq \frac{\mu_L - \mu_R}{eT} \frac{1}{S} \leq \eta_c. \quad (22)$$

Note that, the Seebeck coefficient S is always positive in the engine regime.

Very recently, another tighter bound on engine's efficiency was obtained in Ref. [54, 65] by identifying the input and output currents and imposing conditions on the direction of these current such that the thermoelectric setup operates as an engine. This bound, in our context translates to

$$\langle \eta \rangle \leq \frac{\mu_L - \mu_R}{eT} \frac{1}{S} \sqrt{\frac{ZT}{ZT+1}} \leq \eta_c. \quad (23)$$

Since $ZT > 0$, we arrive to an important conclusion that the bound predicted by Eq. (23) is always tighter than the one given in Eq. (22). In Fig. 10 we asses the bounds in Eq. (23) for the AAH model in presence of the probes as a function of γ and for different λ values. Denoting $\eta_B = \frac{\mu_L - \mu_R}{eT} \frac{1}{S} \sqrt{\frac{ZT}{ZT+1}}$, we show that $\langle \eta \rangle - \eta_B$ and $\eta_B - \eta_c$ are always negative in the parameter regimes considered here. Thus, we find that the bounds in Eq. (23) derived in the linear response regime are valid even in presence of the probes.

V. SUMMARY

In summary, we have investigated the transport properties in quasi-periodic systems in presence of both voltage and voltage-temperature probes. We observe that in all the no-transport regimes the conductance gets enhanced once probes are attached weakly with the sys-

tem and increases with a power-law scaling with the coupling strength. In contrast, for all the Fermi energies where transport takes place in absence of probes, the conductance shows non-monotonic behavior. This feature is observed as long as the probe coupling strength is comparable to other model parameters. Beyond this limit, with increasing probe coupling strength, the conductance becomes independent of the Fermi energies and interestingly follows a power law decay with the coupling strength. This power law scaling observed here turns out to be different from what was reported in a recent work following the local Lindblad master equation approach [34]. This further pin points that, the two different approaches namely NEGF and local Lindblad master equation, effectively mimic different underlying scattering processes. For sufficiently strong coupling, the transport eventually becomes diffusive in all regimes of the original model and in fact the conductance properties become independent of the value of quasi-periodic lattice strength. However, with finite but small probe coupling, a crossover from coherent transport to diffusive transport can be observed. Such crossover length is insensitive to the temperature but depends crucially on the transport regime of the original model.

We also investigated the thermoelectric properties of the AAH model by incorporating voltage-temperature probes and further assessed, in presence of probes, the validity of two recently obtained tighter bounds on thermoelectric engine efficiency and also showed that the bound obtained following Ref. [54] is always tighter than the one predicted by the TUR.

ACKNOWLEDGEMENT

The authors would like to acknowledge Archak Purkayastha for numerous useful discussions. M. S acknowledges funding from National Postdoctoral Fellowship Scheme (NPDF), SERB file no. PDF/2020/000992. B. P. V. is supported by a Department of Science & Technology Science and Engineering Research Board (India) Start-up Research Grant No. SRG/2019/001585. BKA acknowledges the MATRICES grant MTR/2020/000472 from SERB, Government of India and the Shastri Indo-Canadian Institute for providing financial support for this research work in the form of a Shastri Institutional Collaborative Research Grant (SICRG).

[1] S. Aubry and G. André, Ann. Israel Phys. Soc. **3**, 133 (1980).
[2] P. G. Harper, Proceedings of the Physical Society. Section A **68**, 874 (1955).
[3] S. Ganeshan, K. Sun, and S. Das Sarma, Phys. Rev. Lett. **110**, 180403 (2013).
[4] S. Ganeshan, J. H. Pixley, and S. Das Sarma, Phys. Rev. Lett. **114**, 146601 (2015).

[5] S. Ostlund, R. Pandit, D. Rand, H. J. Schellnhuber, and E. D. Siggia, *Phys. Rev. Lett.* **50**, 1873 (1983).

[6] J. Sutradhar, S. Mukerjee, R. Pandit, and S. Banerjee, *Phys. Rev. B* **99**, 224204 (2019).

[7] R. Modak and S. Mukerjee, *Phys. Rev. Lett.* **115**, 230401 (2015).

[8] J.-y. Choi, S. Hild, J. Zeiher, P. Schauß, A. Rubio-Abadal, T. Yefsah, V. Khemani, D. A. Huse, I. Bloch, and C. Gross, *Science* **352**, 1547 (2016).

[9] Y. E. Kraus, Y. Lahini, Z. Ringel, M. Verbin, and O. Zilberberg, *Phys. Rev. Lett.* **109**, 106402 (2012).

[10] M. Verbin, O. Zilberberg, Y. E. Kraus, Y. Lahini, and Y. Silberberg, *Phys. Rev. Lett.* **110**, 076403 (2013).

[11] F. A. An, K. Padavić, E. J. Meier, S. Hegde, S. Ganeshan, J. H. Pixley, S. Vishveshwara, and B. Gadway, (2020), arXiv:2007.01393.

[12] H. P. Lüschen, S. Scherg, T. Kohlert, M. Schreiber, P. Bordia, X. Li, S. Das Sarma, and I. Bloch, *Phys. Rev. Lett.* **120**, 160404 (2018).

[13] H. P. Lüschen, P. Bordia, S. S. Hodgman, M. Schreiber, S. Sarkar, A. J. Daley, M. H. Fischer, E. Altman, I. Bloch, and U. Schneider, *Phys. Rev. X* **7**, 011034 (2017).

[14] M. Atala, M. Aidelsburger, M. Lohse, J. T. Barreiro, B. Paredes, and I. Bloch, *Nature Physics* **10**, 588 (2014).

[15] Y. Lahini, R. Pugatch, F. Pozzi, M. Sorel, R. Morandotti, N. Davidson, and Y. Silberberg, *Phys. Rev. Lett.* **103**, 013901 (2009).

[16] T. Kohlert, S. Scherg, X. Li, H. P. Lüschen, S. Das Sarma, I. Bloch, and M. Aidelsburger, *Phys. Rev. Lett.* **122**, 170403 (2019).

[17] V. Balachandran, S. R. Clark, J. Goold, and D. Poletti, *Phys. Rev. Lett.* **123**, 020603 (2019).

[18] C. Chiaracane, M. T. Mitchison, A. Purkayastha, G. Haack, and J. Goold, *Phys. Rev. Research* **2**, 013093 (2020).

[19] M. Saha and S. K. Maiti, *Journal of Physics D: Applied Physics* **52**, 465304 (2019).

[20] M. Saha and S. K. Maiti, *Physica E: Low-dimensional Systems and Nanostructures* **93**, 275 (2017).

[21] S. Ostlund, R. Pandit, D. Rand, H. J. Schellnhuber, and E. D. Siggia, *Phys. Rev. Lett.* **50**, 1873 (1983).

[22] M. Kohmoto, B. Sutherland, and C. Tang, *Phys. Rev. B* **35**, 1020 (1987).

[23] A. Purkayastha, A. Dhar, and M. Kulkarni, *Phys. Rev. B* **96**, 180204 (2017).

[24] A. Purkayastha, S. Sanyal, A. Dhar, and M. Kulkarni, *Phys. Rev. B* **97**, 174206 (2018).

[25] M. Saha, S. K. Maiti, and A. Purkayastha, *Phys. Rev. B* **100**, 174201 (2019).

[26] M. Saha, B. K. Agarwalla, and B. P. Venkatesh, *Phys. Rev. A* **103**, 023330 (2021).

[27] V. K. Varma, C. de Matalier, and M. Žnidarič, *Phys. Rev. E* **96**, 032130 (2017).

[28] M. Žnidarič and M. Ljubotina, *Proceedings of the National Academy of Sciences* **115**, 4595 (2018).

[29] V. K. Varma and M. Žnidarič, *Phys. Rev. B* **100**, 085105 (2019).

[30] M. Žnidarič and M. Horvat, *The European Physical Journal B* **86**, 67 (2013).

[31] M. V. Medvedyeva, T. c. v. Prosen, and M. Žnidarič, *Phys. Rev. B* **93**, 094205 (2016).

[32] M. Žnidarič, J. J. Mendoza-Arenas, S. R. Clark, and J. Goold, *Annalen der Physik* **529**, 1600298 (2017).

[33] M. Žnidarič, *Phys. Rev. B* **97**, 214202 (2018).

[34] A. M. Lacerda, J. Goold, and G. T. Landi, *Phys. Rev. B* **104**, 174203 (2021).

[35] D. Dwiputra and F. P. Zen, *Phys. Rev. A* **104**, 022205 (2021).

[36] C. Chiaracane, A. Purkayastha, M. T. Mitchison, and J. Goold, arXiv preprint arXiv:2112.02035 (2021).

[37] E. Zerah-Harush and Y. Dubi, *Phys. Rev. Research* **2**, 023294 (2020).

[38] M. Büttiker, *Phys. Rev. B* **32**, 1846 (1985).

[39] M. Büttiker, *Phys. Rev. B* **33**, 3020 (1986).

[40] S. Pilgram, P. Samuelsson, H. Förster, and M. Büttiker, *Phys. Rev. Lett.* **97**, 066801 (2006).

[41] H. Förster, P. Samuelsson, S. Pilgram, and M. Büttiker, *Phys. Rev. B* **75**, 035340 (2007).

[42] C. J. Cattena, R. A. Bustos-Marún, and H. M. Pastawski, *Phys. Rev. B* **82**, 144201 (2010).

[43] D. Nozaki, C. Gomes da Rocha, H. M. Pastawski, and G. Cuniberti, *Phys. Rev. B* **85**, 155327 (2012).

[44] J. Maassen, F. Zahid, and H. Guo, *Phys. Rev. B* **80**, 125423 (2009).

[45] D. Nozaki, Y. Girard, and K. Yoshizawa, *The Journal of Physical Chemistry C* **112**, 17408 (2008).

[46] M. Kilgour and D. Segal, *The Journal of Chemical Physics* **144**, 124107 (2016).

[47] M. Kilgour and D. Segal, *The Journal of Chemical Physics* **143**, 024111 (2015).

[48] R. Korol, M. Kilgour, and D. Segal, *Computer Physics Communications* **224**, 396 (2018).

[49] M. Bandyopadhyay and D. Segal, *Phys. Rev. E* **84**, 011151 (2011).

[50] S. Bedikhal, M. Bandyopadhyay, and D. Segal, *The European Physical Journal B* **86**, 506 (2013).

[51] J. L. D'Amato and H. M. Pastawski, *Phys. Rev. B* **41**, 7411 (1990).

[52] D. Roy, *Journal of Physics: Condensed Matter* **20**, 025206 (2007).

[53] D. Roy and A. Dhar, *Phys. Rev. B* **75**, 195110 (2007).

[54] S. Saryal, M. Gerry, I. Khait, D. Segal, and B. K. Agarwalla, *Phys. Rev. Lett.* **127**, 190603 (2021).

[55] P. Pietzonka and U. Seifert, *Phys. Rev. Lett.* **120**, 190602 (2018).

[56] J. Schwinger, *Journal of Mathematical Physics* **2**, 407 (1961).

[57] L. V. Keldysh, *Diagram technique for nonequilibrium processes* (1964).

[58] J. Rammer and H. Smith, *Rev. Mod. Phys.* **58**, 323 (1986).

[59] H. Haug and A. Jauho, *Quantum Kinetics in Transport and Optics of Semiconductors* (Springer, New York, 2008).

[60] J.-S. Wang, B. K. Agarwalla, H. Li, and J. Thingna, *Frontiers of Physics* **9**, 673 (2014).

[61] Y. Meir and N. S. Wingreen, *Phys. Rev. Lett.* **68**, 2512 (1992).

[62] A. Dhar and D. Sen, *Phys. Rev. B* **73**, 085119 (2006).

[63] A. C. Barato and U. Seifert, *Phys. Rev. Lett.* **114**, 158101 (2015).

[64] T. R. Gingrich, J. M. Horowitz, N. Perunov, and J. L. England, *Phys. Rev. Lett.* **116**, 120601 (2016).

[65] S. Mohanta, S. Saryal, and B. K. Agarwalla, arXiv preprint arXiv:2106.12809 (2021).